MICROCOPY RESOLUTION TEST CHART
NATIONAL BUREAU OF STANDARDS-1963-A

AD-A173 541

Hydrodynamic Aspects of
the Split-Foil Laser Target Design

JILL P. DAHLBURG, JOHN H. GARDNER, MARK H. EMERY, AND JAY P. BORIS

Laboratory for Computational Physics

DTIC
ELECTE
OCT 2 4 1986
B

DTIC FILE COPY

86 1

REPORT DOCUMENTATION PAGE

1a. REPORT SECURITY CLASSIFICATION UNCLASSIFIED			1b. RESTRICTIVE MARKINGS			
2a. SECURITY CLASSIFICATION AUTHORITY			3. DISTRIBUTION/AVAILABILITY OF REPORT			
2b. DECLASSIFICATION/DOWNGRADING SCHEDULE			Approved for public release, distribution unlimited			
4. PERFORMING ORGANIZATION REPORT NUMBER(S) NRL Memorandum Report 5839			5. MONITORING ORGANIZATION REPORT NUMBER(S)			
6a. NAME OF PERFORMING ORGANIZATION Naval Research Laboratory	6b. OFFICE SYMBOL (If applicable) Code 4040		7a. NAME OF MONITORING ORGANIZATION Department of Energy			
6c. ADDRESS (City, State, and ZIP Code) Washington, DC 20375-5000			7b. ADDRESS (City, State, and ZIP Code) Washington, DC			
8a. NAME OF FUNDING/SPONSORING ORGANIZATION Department of Energy	8b. OFFICE SYMBOL (If applicable)		9. PROCUREMENT INSTRUMENT IDENTIFICATION NUMBER			
8c. ADDRESS (City, State, and ZIP Code) Washington, DC 20545			10. SOURCE OF FUNDING NUMBERS			

PROGRAM ELEMENT NO.	PROJECT NO.	TASK NO.	WORK UNIT ACCESSION NO.
DOE	DOE	81425	DN155-384

11. TITLE (Include Security Classification)

Hydrodynamic Aspects of the Split-Foil Laser Target Design

12. PERSONAL AUTHOR(S)
Dahlburg, Jill P., Gardner, John H., Emery, Mark H., and Boris, Jay P.

13a. TYPE OF REPORT Interim	13b. TIME COVERED FROM _____ TO _____	14. DATE OF REPORT (Year, Month, Day) 17 September 1986	15. PAGE COUNT 25

16. SUPPLEMENTARY NOTATION

17 COSATI CODES			18. SUBJECT TERMS (Continue on reverse if necessary and identify by block number)
FIELD	GROUP	SUB-GROUP	X-ray lasers,
			laser-matter interactions,
			hydrodynamic simulation

19. ABSTRACT (Continue on reverse if necessary and identify by block number)

Hydrodynamic simulations of exploding copper foils, which are irradiated on one side by 1.06 μm laser light, indicated that peak axial electron number density is more easily controlled with the split-foil target design. Results from a series of simulations with solid copper foils that range in width from 500 Å to 1500 Å show that while peak electron temperature and time of burnthrough can be varied, evolved electron number densities are approximately bounded from above by 3×10^{20} particles/cc. By increasing foil thickness to 1 μm and introducing a slit on the foil axis of 100 μm width, uniform plasmas with electron number densities on the order of 6×10^{20} particles/cc can be generated. Essentially the same results are obtained from simulations with split selenium foils.

20. DISTRIBUTION/AVAILABILITY OF ABSTRACT ☒ UNCLASSIFIED/UNLIMITED ☐ SAME AS RPT ☐ DTIC USERS	21. ABSTRACT SECURITY CLASSIFICATION UNCLASSIFIED	
22a. NAME OF RESPONSIBLE INDIVIDUAL Dr. Jill Dahlburg	22b. TELEPHONE (Include Area Code) (202) 767-3055	22c. OFFICE SYMBOL Code 4040

DD FORM 1473, 84 MAR 83 APR edition may be used until exhausted All other editions are obsolete

☆U.S. Government Printing Office: 1985-887-047

i

CONTENTS

DTIC
ELECTE
OCT 2 4 1986

B

Accession For

NTIS GRA&I
DTIC TAB
Unannounced
Justification

By
Distribution/

Availability Codes

Dist	Avail and/or Special
A-1	

QUALITY INSPECTED

HYDRODYNAMIC ASPECTS OF
THE SPLIT-FOIL LASER TARGET DESIGN

I. INTRODUCTION

The generation of uniform electron number densities in neon-like states of high-z plasmas which develop from exploding foils has become a topic of much recent interest. Such plasmas are necessary for the creation of a pumped soft x-ray laser. To date, perhaps the most successful experimental laboratory x-ray laser has been the one designed and operated by Matthews and co-workers at Lawrence Livermore National Laboratory (Matthews *et al* 1984). In these experiments, an amplified x-ray beam is formed when an selenium foil, which is irradiated from both sides for 0.6ns by $0.53\mu m$ laser light, explodes. A uniform cylindrical plasma with electron number densities and temperatures appropriate for x-ray lasing is thereby generated.

It is of interest to generalize these results to other systems and parameter regimes. Of particular promise are the conditions obtainable with the Pharos III laser at the Naval Research Laboratory. In one mode of operation, this laser can provide a single, 500 Joule, $1.06\mu m$ beam, with rise time on the order of 1 ns, and peak laser intensity of approximately $1 \times 10^{13} \frac{W}{cm^2}$. Considerable investigation into the use of this system to generate a pumped soft x-ray laser has been undertaken (Elton *et al* 1986; Lee *et al* 1986). We extend this research by means of numerical simulation, with initial conditions and parameters appropriate to the NRL Pharos III laser operating in its single-sided illumination mode.

We present results from the exploration of a somewhat idealized NRL-like set of regimes in which a measurable x-ray beam can be formed. Sec. II is a discussion of the geometry considered, the assumptions, and the numerical methods used. In Sec. III we discuss results from the simulation of the hydrodynamic evolution of solid copper foils irradiated by a $1.06\mu m$ laser beam, [CASES A - F]. Results from these simulations indicate that the evolved electron number densities decay from an upper bound of approximately 3×10^{20} particles/cc,

1

at approximately 0.25 ns after burnthrough. A promising alternate foil design, the split-foil, is then presented, in Sec. III. It is found that relatively uniform plasmas with electron number densities of 6×10^{20} particles per cc can be generated with $1\mu m$ thick split copper foils, with a slit on axis of width of 0.01 cm. A discussion of these results is then given in Sec. IV.

II. SIMULATION MODEL

The described simulations are performed with the *FAST2D* laser-shell simulation code (Boris, 1976; Boris, 1977; Emery *et al* 1982). The code solves the equations of ideal compressible hydrodynamics in two full dimensions, using the flux-corrected transport algorithm (Boris and Book, 1976). In this code, energy is deposited in the plasma by the incident laser beam through classical inverse bremsstrahlung absorption, and transported through the plasma by classical nonlinear thermal conduction. An adaptive zoning algorithm is employed to insure sufficient resolution in the regions of strong density gradients.

The geometry is identical for all the simulations here described; see Fig. 1. The laser target is assumed to be much longer in the direction of eventual x-ray lasing, the z-direction, and uniform in that direction. This allows the computation to be limited to two-dimensional cross-sections of the exploding foil and to be accurate without sacrificing efficiency. In addition, the problem is assumed to be symmetric about the "vertical" axis, y. The equations thus only need be time-advanced in the upper y half-plane, (the shaded region of Fig. 1a, b), with perfectly reflecting boundary conditions imposed at y = 0. Boundary conditions which simulate unimpeded outward flow of the plasma are imposed at y_{max}. Outflow conditions also are imposed at x_{max}, and at x_{min}. By means of an adaptive gridding algorithm, large buffer zones are constructed at both x_{max} and x_{min}; these buffer zones isolate the important, central region of the mesh, and effectively set x_{edge} to $\pm\infty$. The laser beam is assumed to originate at $x = +\infty$ and the target is centered at x = 0. Typical runs are performed on grids with 120 points parallel to the incident beam (x-direction), and 40 points in the transverse direction (y-direction). In order to resolve the large density gradients, many fine zones of the non-uniform mesh are clustered in the neighborhood of the regions of large density gradients. Since a variable, Courant-limited timestep is used in the calculation, the timestep is thus generally small, of the order of 0.02 ps. The code takes approximately 0.1 second per timestep of CRAY-XMP time, or about 15 minutes for each simulation considered here.

2

Initial conditions for both the solid foil simulations and for the split-foil runs are specified by the one-dimensional quasi-static equilibrium model (Orens, 1980; Manheimer *et al* 1982). In the split-foil cases, the gap is similarly modelled, for code stability, with initial density (x = 0, y = 0) less than critical.

In each case, the material chosen for the foil is pre-ionized to the neon-like state. From evolved densities and temperatures we expect that this is a state the plasma would attain (Rosen *et al* 1984). In addition, the ionization level is held fixed throughout the simulation. This constant Z assumption is computationally efficient. Since the timescales for ionization and recombination vary as the inverse of the density, becoming much longer than relevant hydrodynamic timescales in the expansion phase of the generated plasma (London and Rosen 1986), the assumption is also physically appropriate.

We now turn to a discussion of individual foil cases and results.

III. SOLID FOIL RESULTS

Table 1 lists the runs we have chosen to display here to demonstrate density and temperature states that have evolved from a range of thin, solid copper foils.

For all simulations of this section, the incident laser wavelength is 1.06μm, with a peak intensity that is linearly ramped up for 1 ns, followed by a flat-topped peak intensity, specified for each case. Spatially the pulse is Gaussian, with full-width half-maximum 100μm from the center of the foil.

Since the time of 0.25 ns after burn-through has generally been found to be a time by which the exploded foil's sharp density gradients are no longer observable, it is the time chosen for comparing CASES A-F, as indicated in Figs. 2 - 7. Although a desirably uniform electron density profile has been obtained in each of the six cases by this time, the electron number density in each case's physical plateau region has monotonically decreased to a relatively low value of 3×10^{20} particles / cc. Variation in the initial foil thickness alters the time of burnthrough, and alters, somewhat, the electron temperature in the uniform density region; however, the electron number density evolves to a state which is nearly identical in all cases. See Figs. 3, 5 and 6, and Figs. 2 and 7. Keeping the foil thickness constant and varying the laser intensity again alters burnthrough time and temperature, but does not change the

estimated number density; compare Figs. 2, 3 and 4, and Figs. 6 and 7. We conclude that for thin copper foils that will burn through by approximately 2 ns, with single-sided illumination, the resulting electron number densities are approximately 3×10^{20}. This result is obtained when both peak intensities and initial foil thicknesses are varied. A plasma with a higher plateau electron number density is desirable for greater x-ray gain (Feldman *et al* 1984).

IV. SPLIT-FOIL RESULTS

In order to generate a pumped soft x-ray laser, two qualities are required of the electron number density: (1), the electron plasma must be of sufficient density for x-ray lasing, and (2), a region of uniform density must exist, to minimize refraction losses (Chirkov 1984). Alternate foil designs are thus considered, in an attempt to both raise and enlarge the plateau region electron number density. The simplest case that can be engineered is a thicker foil than that considered in Sec. II. While thicker solid foils would not be feasible if burnthrough by 2 ns is desired, a design geometry that increases the plasma density above that of a flat foil that is only $1500\text{\AA}$ thick is required. By initializing the problem with a $1\mu m$ thick foil which has a slit at the $y = 0$ axis, we find that regions of electron number densities that are both uniform and approximately 6×10^{20} particles/cc can be generated. In addition, the plasma which results from this novel foil design is found to survive in near steady-state for over 1 ns.

For the split-foil simulations considered here, the copper is pre-ionized to the neon-like state, exactly as it was for the solid foils. In addition, the incident laser pulse is identical to that used for the solid copper foil CASE E, with a peak incident laser intensity of $1.00 \times 10^{13} \frac{W}{cm^2}$.

Fig. 8, plots of peak axial electron number density measured at the center of the slit, $n_e(x, y = 0)$, as a function of time, depict the essential result of the split-foil simulations. Fig. 8a, a plot of peak $n_e(x, y = 0)$ *vs* time for a split foil that was initially $10\mu m$ thick, shows a peak electron number density that rises above critical, to stabilize near a value of approximately 1.3×10^{21} particles/cc. Fig. 8b is a similar plot for the $1\mu m$ split foil. In this figure, it is clear that the peak $n_e(x, y = 0)$ hovers near 6×10^{20} particles/cc for longer than 1 ns.

Fig. 9a, a contour plot of n_e from the split-foil case at t $= 1.9 \times 10^{-9}$s, demonstrates how n_e has plateaued in the initially split region, with approximately 6×10^{20} particles / cc. The plateau region is approximately $100\mu m$ in the x direction by $80\mu m$ in y ($40\mu m$ in

4

the half-plane). A contour plot of electron temperature, Fig. 9b, shows that at this time the temperature in the split region is approximately 600 eV. Note the uniform density region across which a uniform, controlled temperature gradient appears. This should be useful for calibrating the lasing models.

To check the sensitivity of our results to material variation, we also performed simulations with selenium. For a given temperature, the ratio of the hydrodynamic pressure to the mass density essentially depends on the ratio of a target's ionization level, Z, to its atomic mass, A. Thus, once a plasma has been generated and heated by the incident laser beam, the hydrodynamic evolution that plasma undergoes will be governed by the ratio Z/A. For a rather wide range of materials of interest this ratio is nearly constant. For instance, the ratio Z/A for copper ionized to the neon-like state is 0.299. The ratio Z/A for selenium ionized to the neon-like state is 0.303. From this similarity, it may be expected that results from simulations with selenium ionized to the neon-like state will be nearly identical to results from the above described simulations with copper. We find this to be the case; results from a simulation performed with a pre-ionized split selenium foil that initially was $1\mu m$ thick are very similar to those obtained with copper foils. The incident laser pulse used in the selenium simulation is spatially uniform, and is temporally identically to that specified for CASE E. Fig. 10a, a plot of peak axial $n_e(x, y = 0)$ vs time for the split selenium foil demonstrates that the hydrodynamic evolution of the resulting plasma is very similar to that generated from copper. Fig. 10b is a snapshot, at $t = 1.125 \times 10^{-9}$s, of the electron number density which has developed from the $1\mu m$ thick split selenium foil. This figure shows the large axial region of uniform density which has been formed from the ablating selenium foil, a result which is nearly identical to results obtained from copper foils.

V. DISCUSSION

We have performed numerical simulations of two distinct copper foil target designs. In all the cases simulated, the exploding thin solid copper foils with single-sided illumination generate somewhat uniform electron number densities which are approximately bounded from above by 3×10^{20} particles/cc. This low number density in the physical plateau region is obtained even when the initial target foil is thickened by a factor of two.

5

Plateau-region plasma electron number densities can be varied, however, as simulations with ablating split copper foils demonstrate. For $10\mu m$ split copper foils, super-critical axial densities are achieved. From ablating split copper foils that are initially $1\mu m$ thick, approximately $100\mu m$ plasmas with relatively flat electron number densities of approximately 6×10^{20} particles / cc are generated. This higher density plasma is found to exist, in near steady-state, for over 1 ns. A key to understanding the reason for the development of a nearly steady-state situation can be found in the behavior of the plasma flow.

Two evolved velocity fields are depicted in Fig. 11. Fig. 11a is the flow pattern for the solid copper foil CASE E at $t = 2.12 \times 10^{-9}$s. Fig. 11b is the flow pattern at $t = 1.9 \times 10^{-9}$s for the $1\mu m$ split copper foil simulation. The incident laser pulse is identical in each case. A dynamical explanation for the difference in peak axial electron number densities which results from the foil shape may be obtained from this pair of figures. In the solid foil case, a flow field is set up that can only convect the plasma rapidly away from the region of interest. On the other hand, from Fig. 11b it is clear that a nearly steady-state situation has evolved in the split-foil case. As on-axis plasma is swept away to $x = \pm\infty$ a nearly equal amount is steadily ablated into the neighborhood of the axis from the relatively infinite solid copper reservoir, the split-foil. The pressure and density are higher in the split foil case because the vertical velocity must be stagnated and because the mass available will only depend weakly on the pulse intensity. This steady-state situation is found to be robust, as is shown by Fig. 8b. In this steady situation, the plasma which streams away from the potential lasing region is continually replaced by plasma that is fed into the region from the ablating foil. This evolution is also observed in hydrodynamic simulations of split selenium foils.
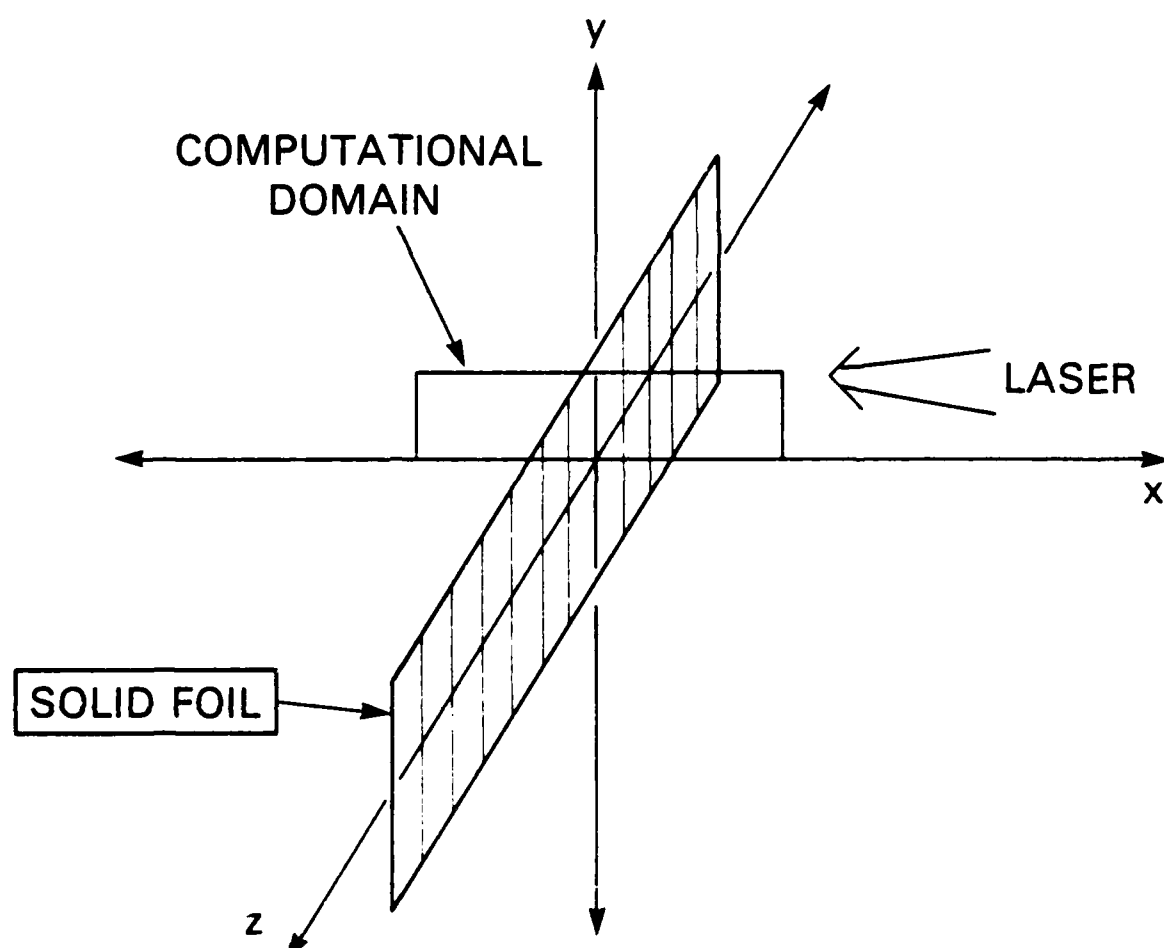
Thus, by means of this new target foil design, we find that generated plasma densities may be controlled, both as a function of time and of space.

TABLE I

Solid copper foil runs

CASE	$I_{max}, \frac{W}{cm^2}$	Width (Å)	$t_{crit} \times 10^{-9}s$	T (eV)
A	1.50×10^{13}	7.5×10^2	0.89	800
B	1.00×10^{13}	7.5×10^2	1.04	720
C	0.75×10^{13}	7.5×10^2	1.22	640
D	1.00×10^{13}	1.0×10^3	1.31	720
E	1.00×10^{13}	1.5×10^3	1.88	760
F	1.50×10^{13}	1.5×10^3	1.54	850

(a) Solid-foil computational domain

Fig. 1 — Simulation geometry
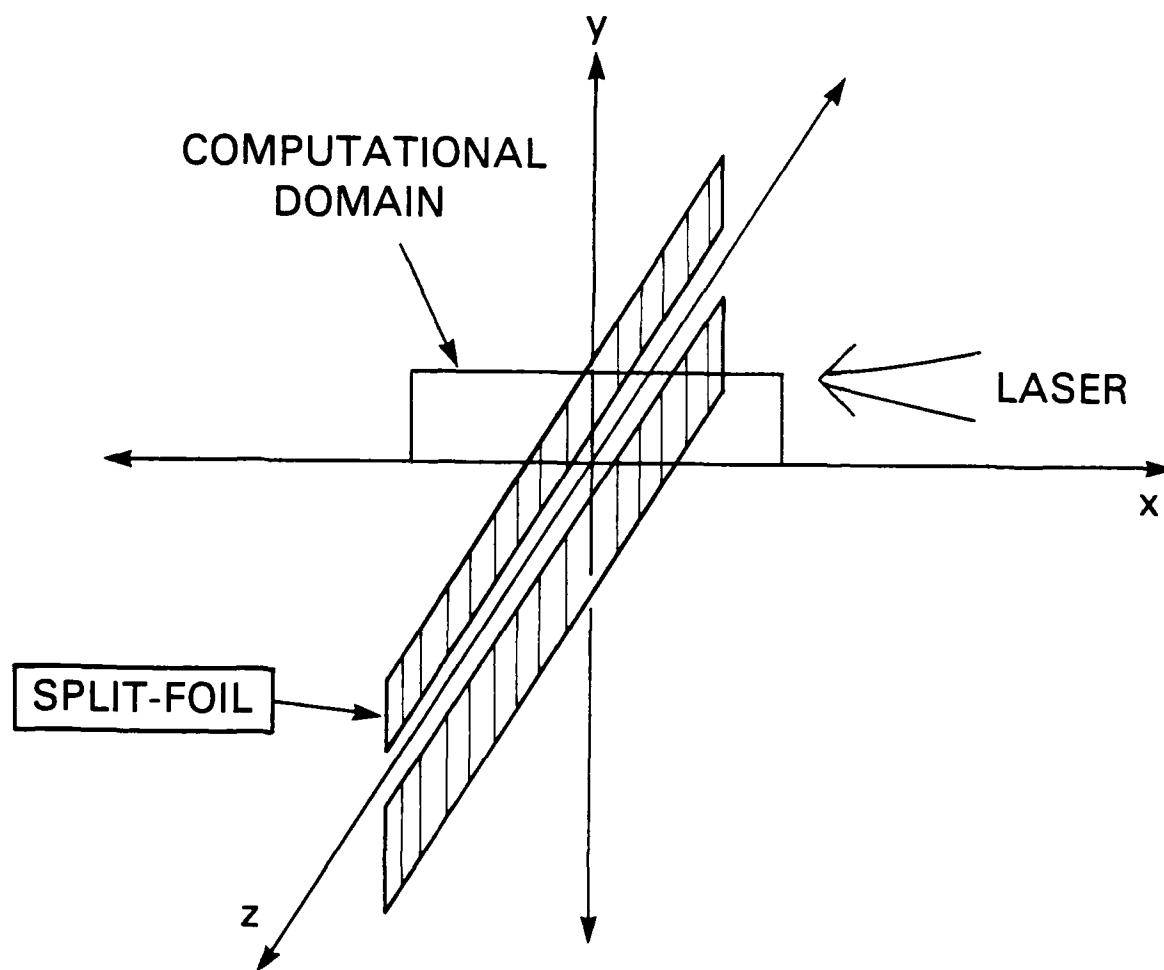
(b) Split-foil computational domain

Fig. 1 (Continued) — Simulation geometry

n_e (x,y,t=1.125×10^{-9} s)

(a) Contours of constant $n_e/10^{20}$

T_{ev} (x,y,t=1.125×10^{-9} s)
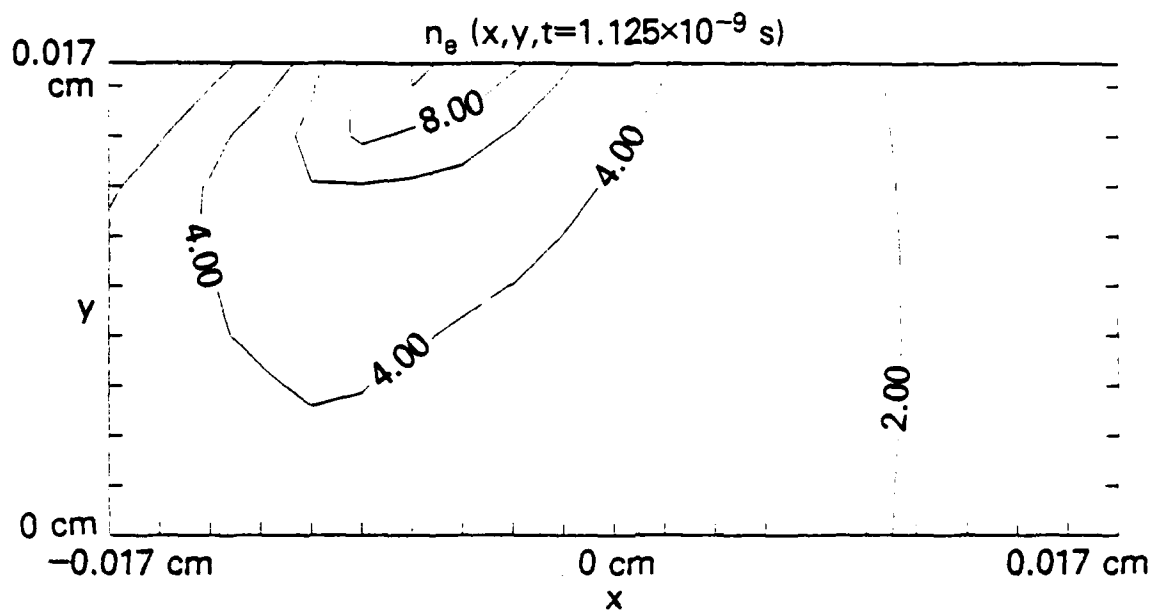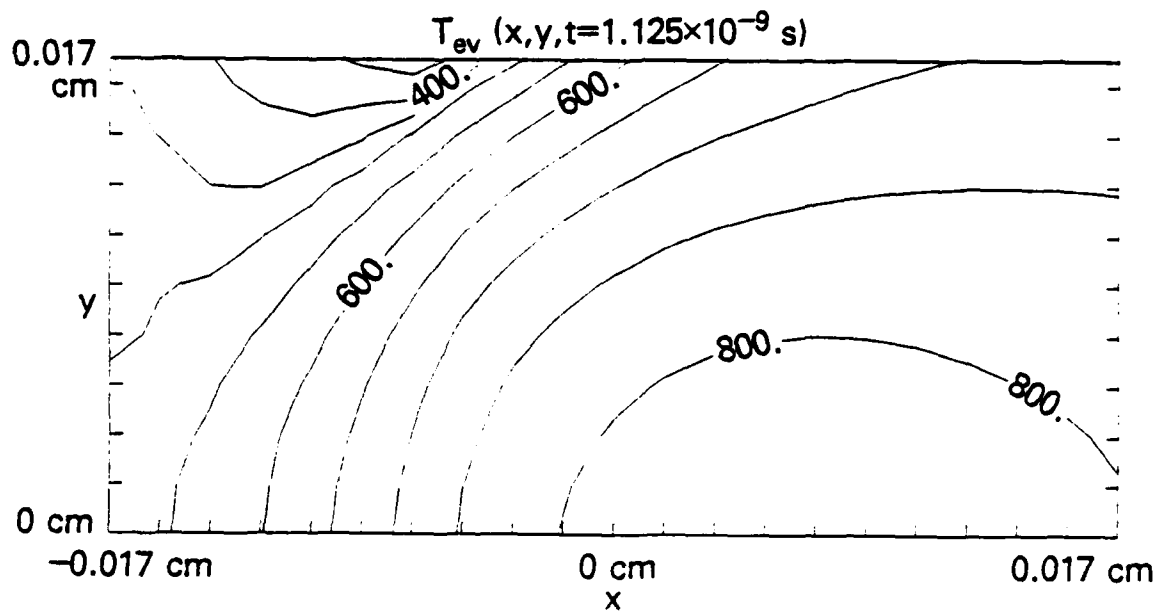
(b) Contours of constant temperature, in eV

Fig. 2 — Thin solid foil, CASE A, at $t = 1.125 \times 10^{-9}$s

10

n_e $(x, y, t = 1.28 \times 10^{-9}$ s$)$

0.017 cm

y

0 cm

−0.017 cm   0 cm   0.017 cm

x

(a) Contours of constant $n_e / 10^{20}$

T_{ev} $(x, y, t = 1.28 \times 10^{-9}$ s$)$

0.017 cm

y

0 cm

−0.017 cm   0 cm   0.017 cm

x
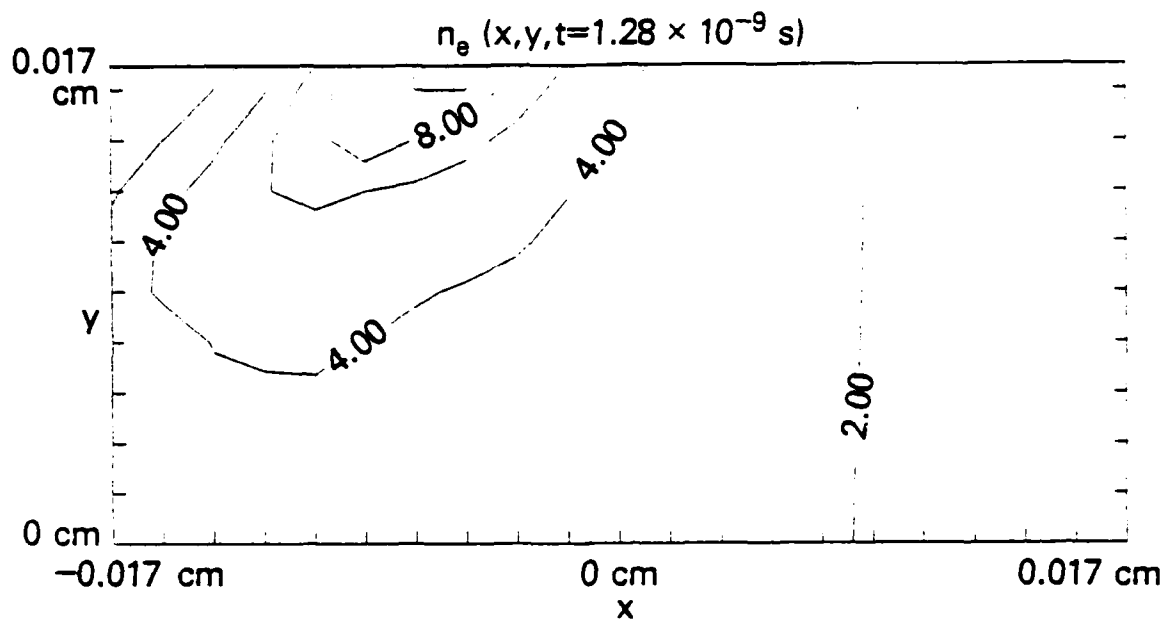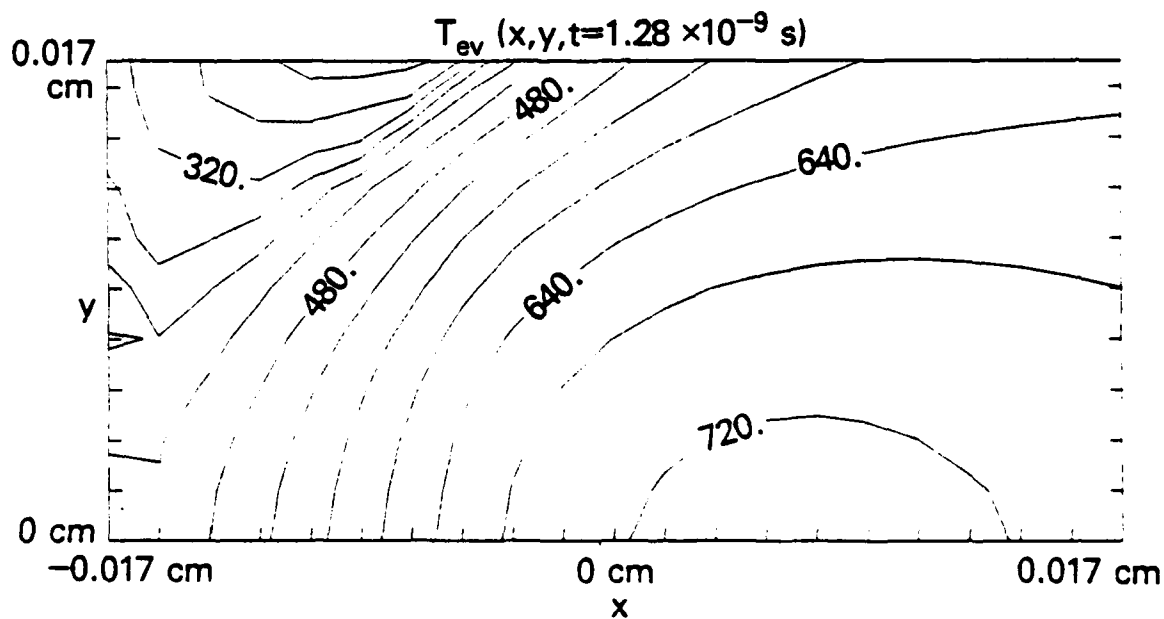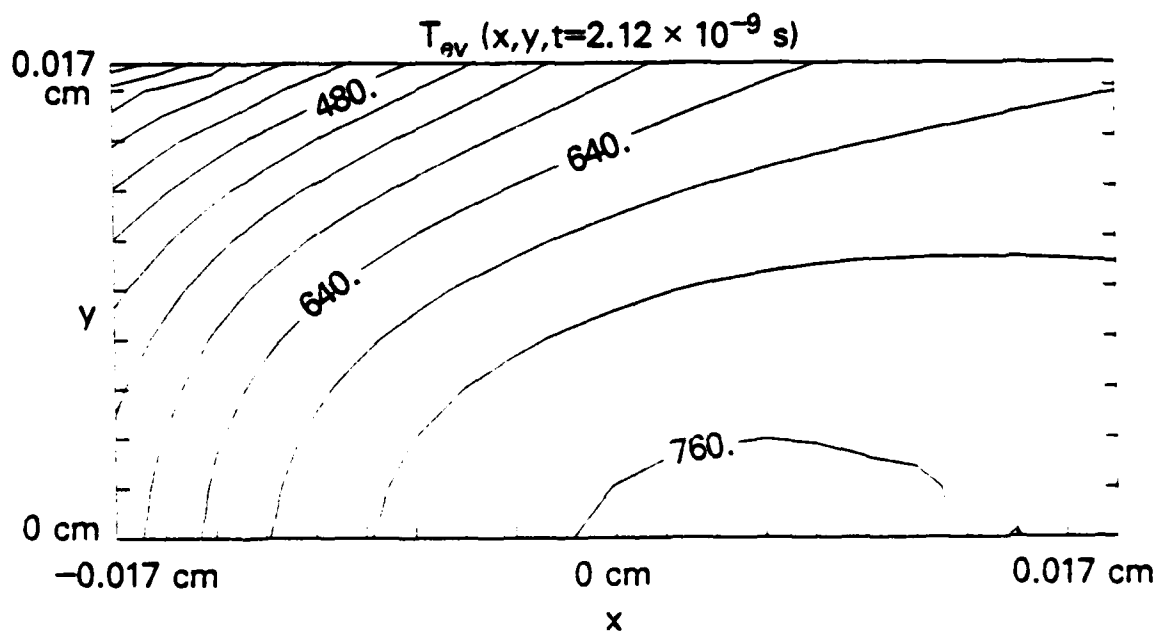
(b) Contours of constant temperature, in eV

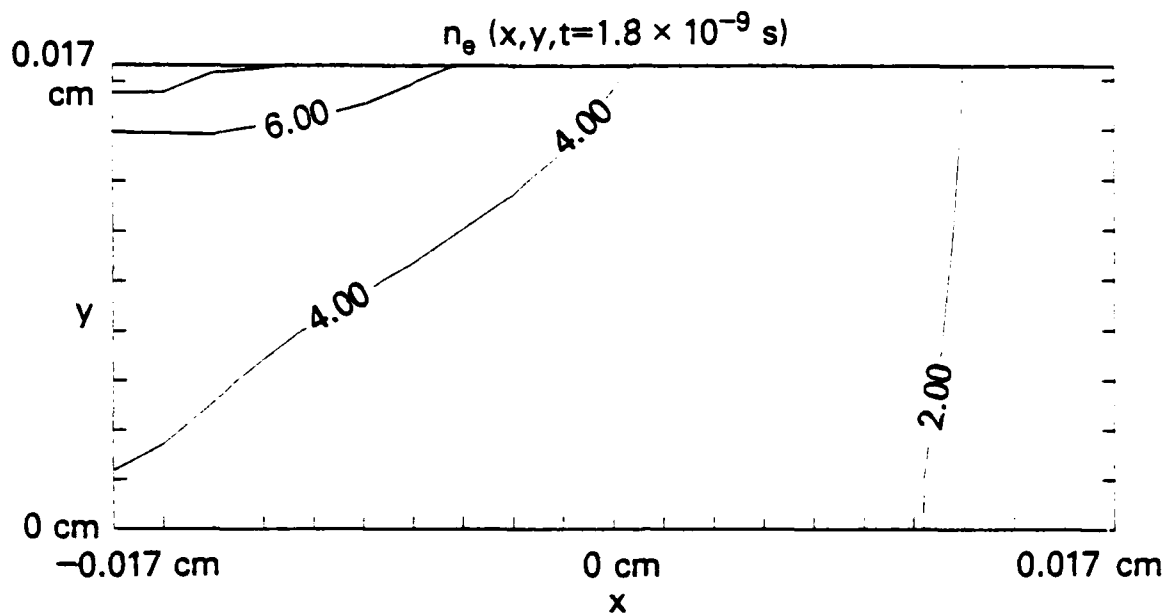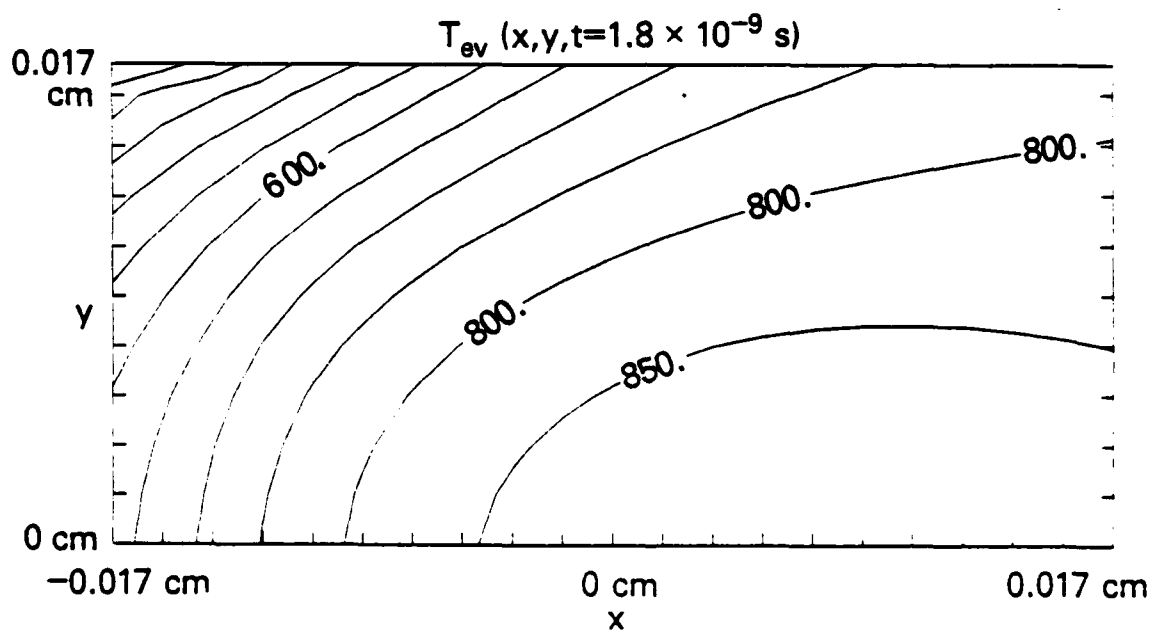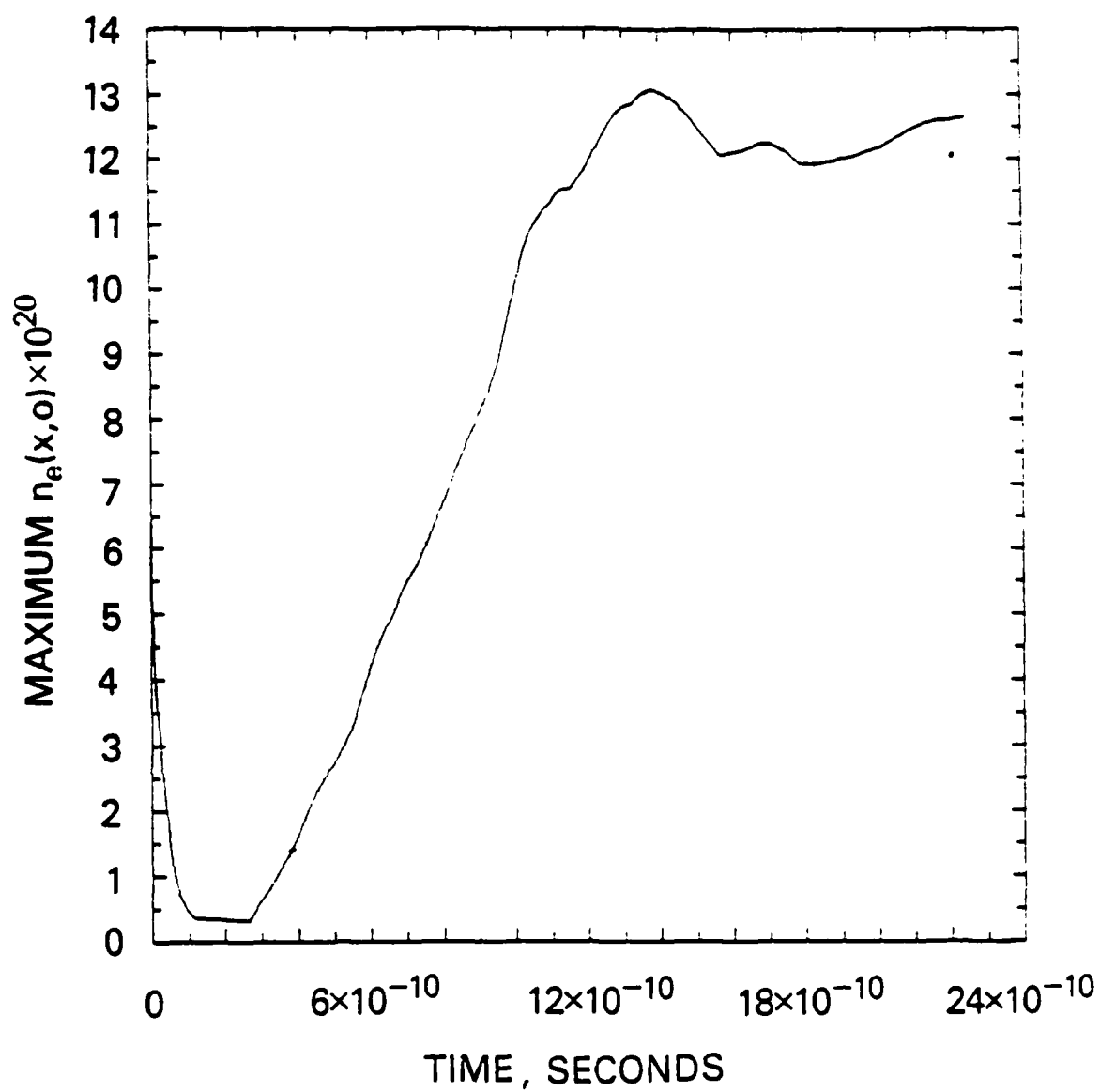Fig. 3 — Thin solid foil, CASE B, at $t = 1.28 \times 10^{-9}$s

11
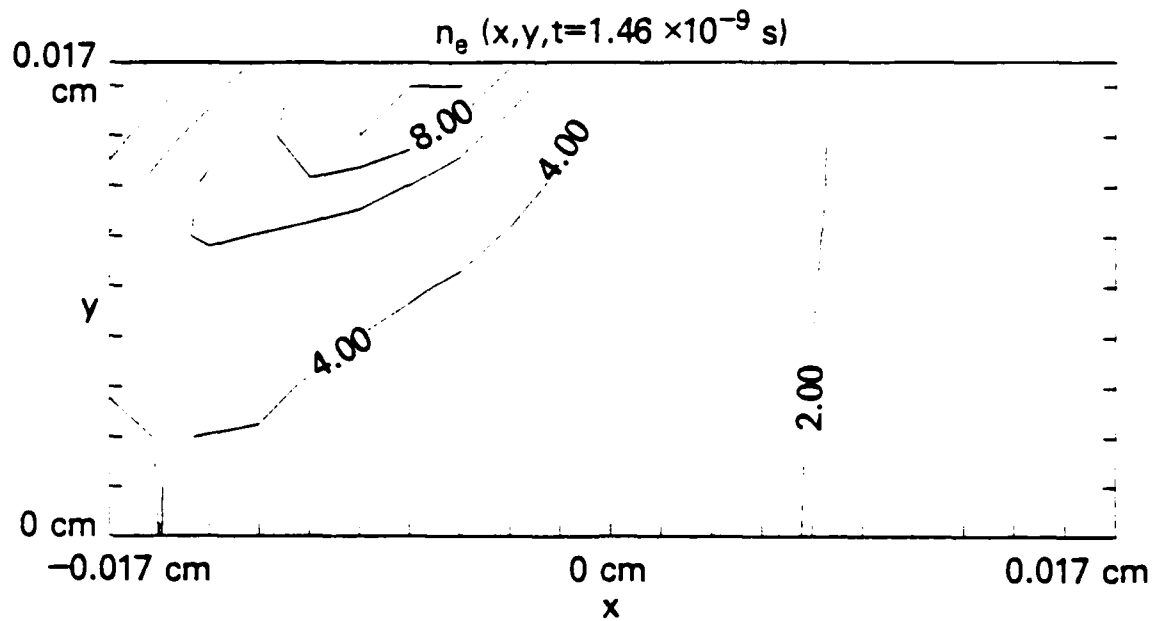
(a) Contours of constant $n_e/10^{20}$
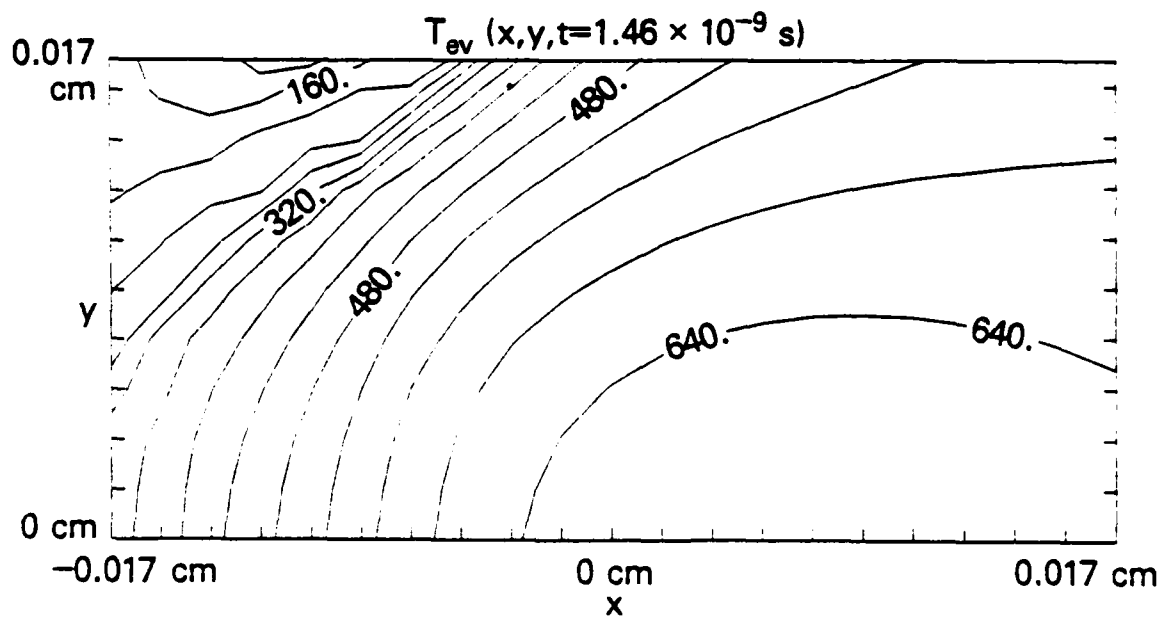
(b) Contours of constant temperature, in eV

Fig. 4 — Thin solid foil, CASE C, at $t = 1.46 \times 10^{-9}$s

n_e (x,y,t=1.55 × 10^{-9} s)

(a) Contours of constant, $n_e/10^{20}$

T_{ev} (x,y,t=1.55 × 10^{-9}s)
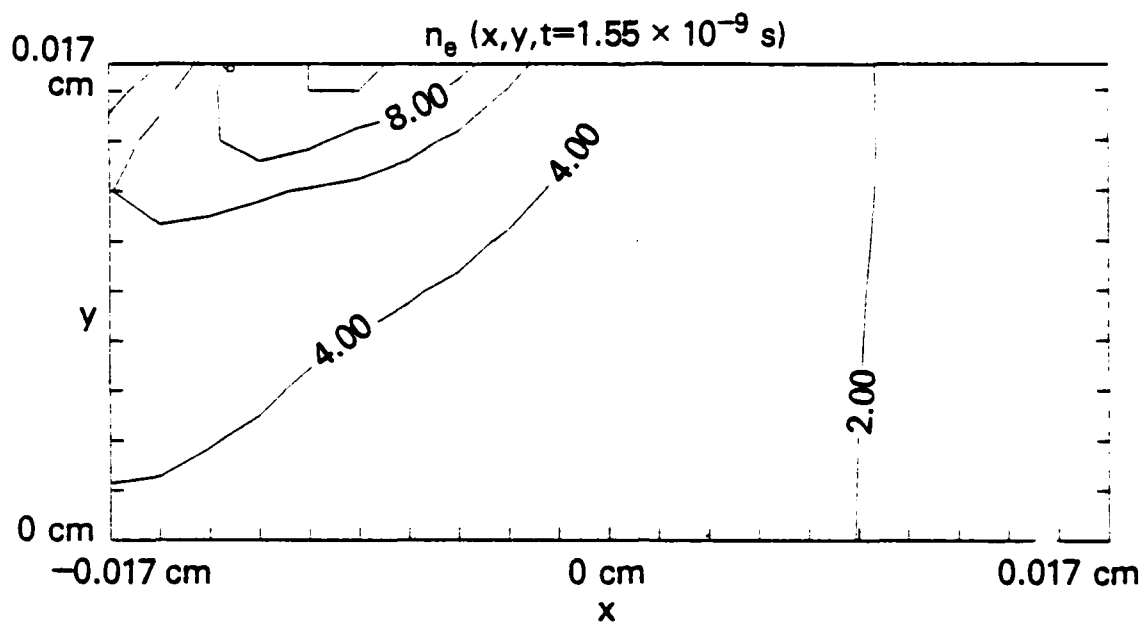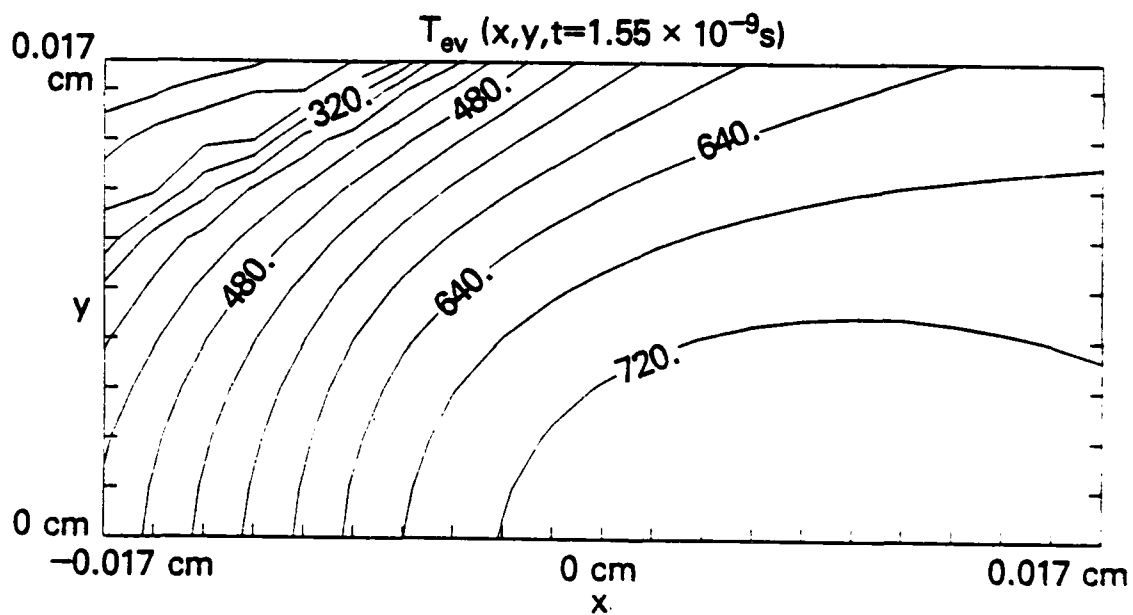
(b) Contours of constant temperature, in eV

Fig. 5 — Thin solid foil, CASE D, at t = 1.55 × 10^{-9}s

n_e $(x, y, t = 2.12 \times 10^{-9}$ s$)$

6.00

4.00

4.00

2.00

0.017 cm

y

0 cm

−0.017 cm   0 cm   0.017 cm

x

(a) Contours of constant $n_e / 10^{20}$

T_{ev} $(x, y, t = 2.12 \times 10^{-9}$ s$)$

480.

640.

640.

760.

0.017 cm

y

0 cm

−0.017 cm   0 cm   0.017 cm

x
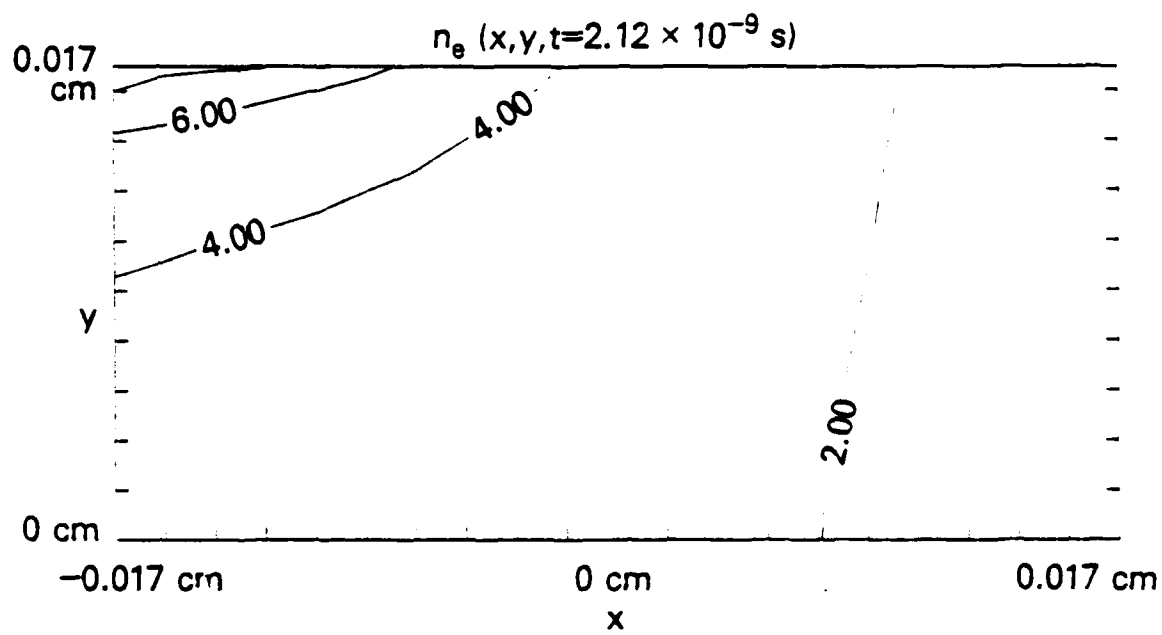
(b) Contours of constant temperature, in eV

Fig. 6 — Thin solid foil, CASE E, at $t = 2.12 \times 10^{-9}$s

14

n_e (x,y,t=1.8 × 10^{-9} s)

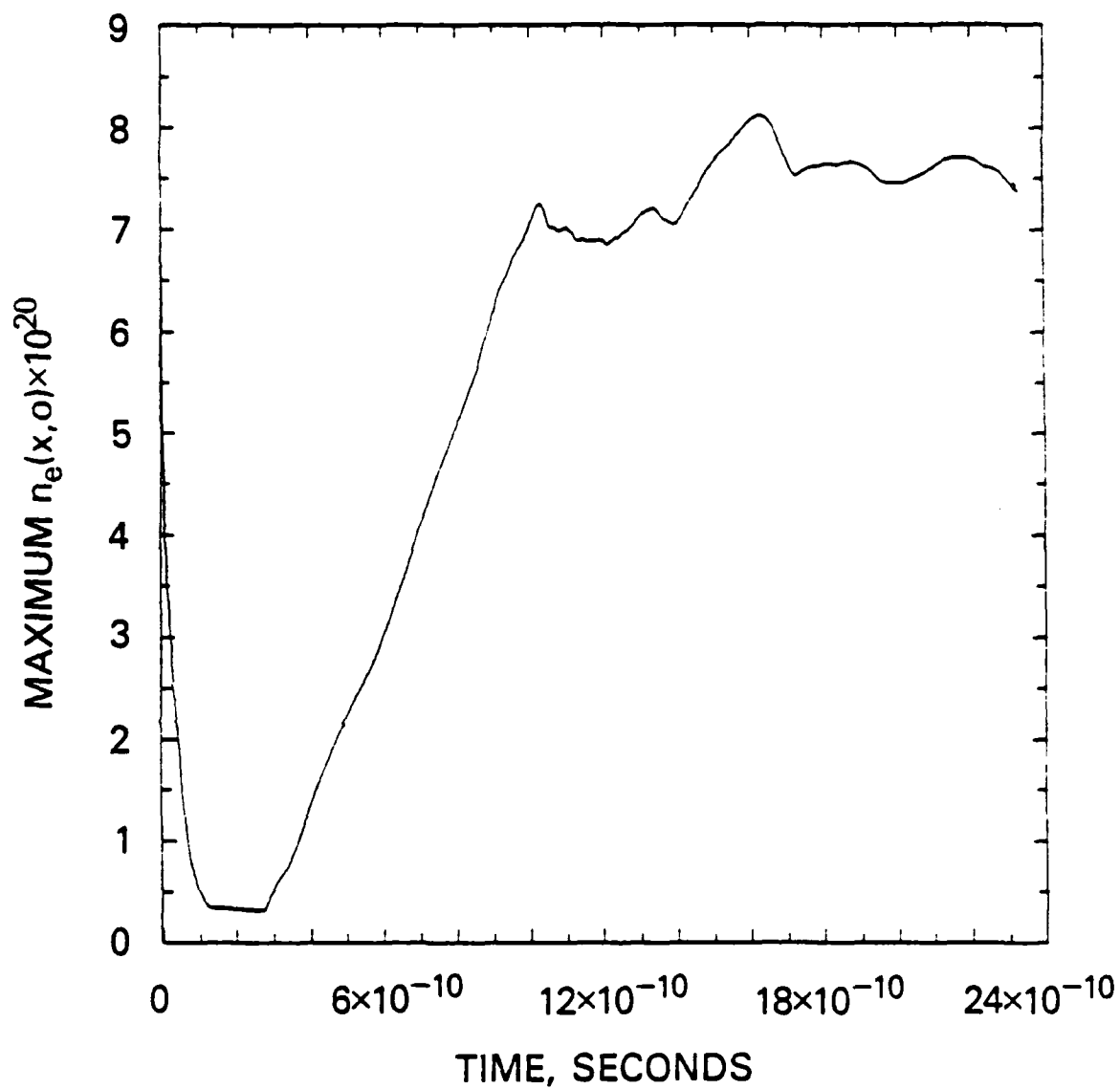(a) Contours of constant $n_e/10^{20}$

T_{ev} (x,y,t=1.8 × 10^{-9} s)

(b) Contours of constant temperature, in eV

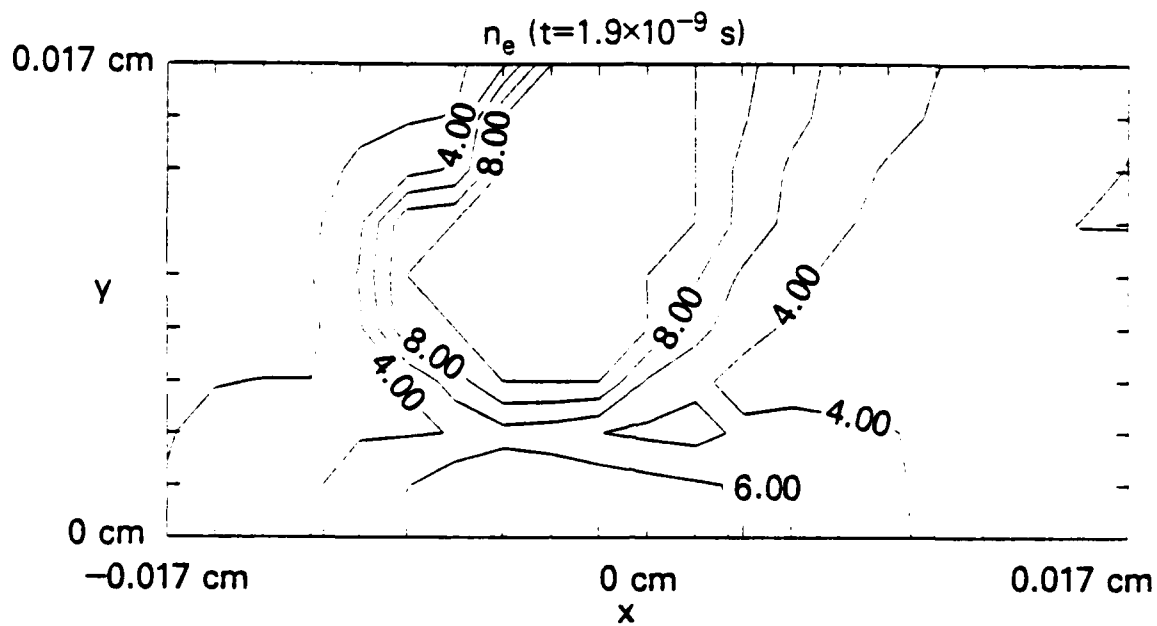Fig. 7 — Thin solid foil, CASE F, at $t = 1.8 \times 10^{-9}$s

15

(a) Initial foil thickness of 10 μm

Fig. 8 — Peak axial electron number density as a function of time.
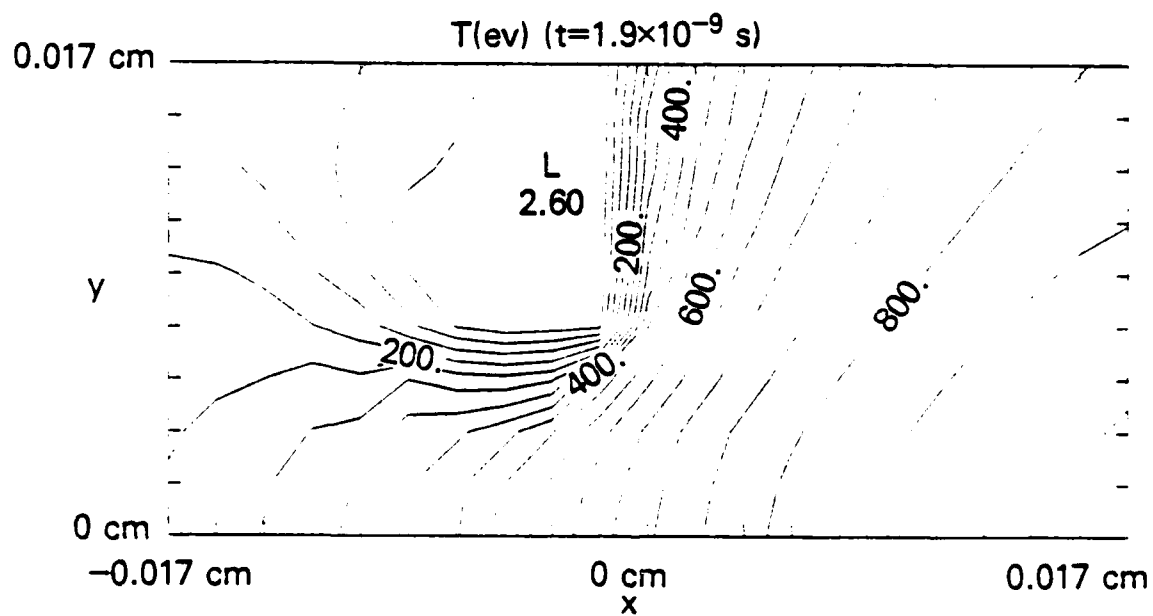for the split copper foil cases

(b) Initial foil thickness of $1\mu m$

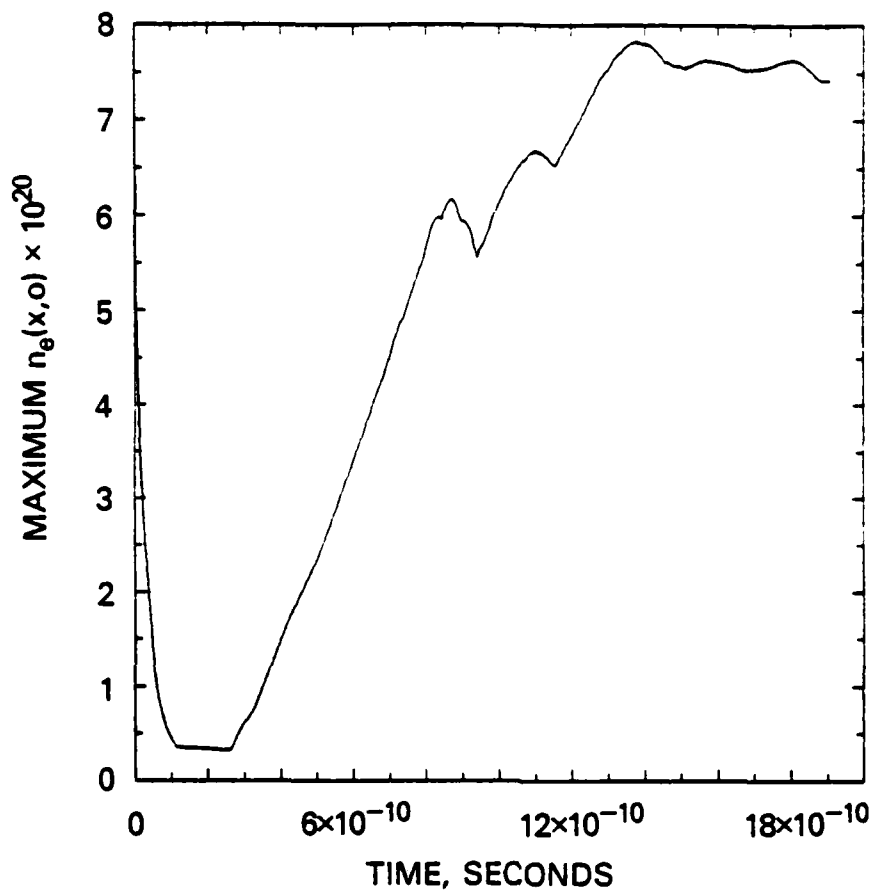Fig. 8 (Continued) — Peak axial electron number density as a function of time, for the split copper foil cases
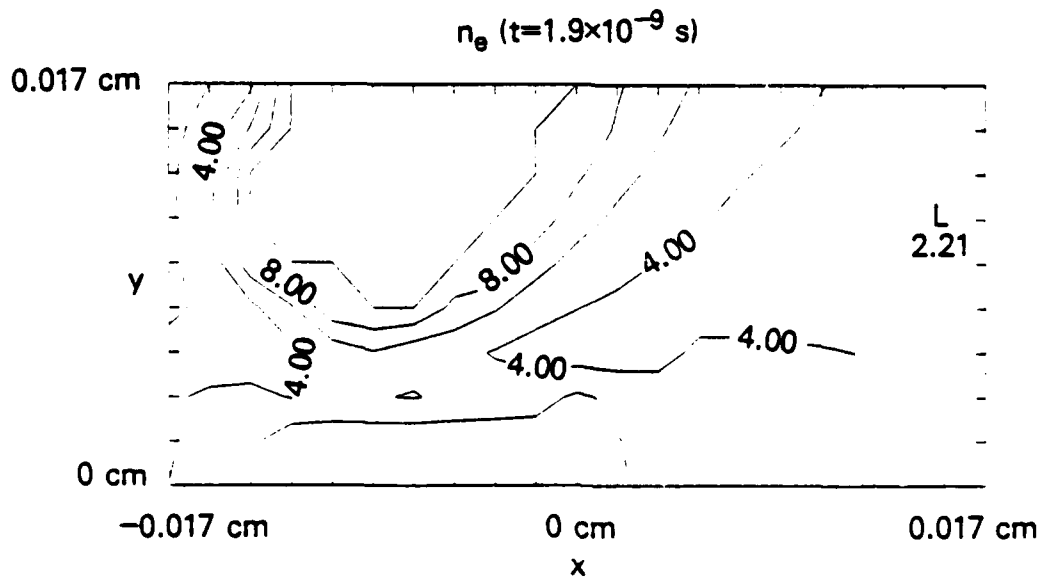
(a) Contours of constant $n_e/10^{20}$

(b) Contours of constant temperature, in eV

Fig. 9 — $1\mu m$ split copper foil, at a time 1.9×10^{-9}s

(a) Peak axial electron number density as a function of time

n_e ($t=1.9\times10^{-9}$ s)

(b) Contours of constant $n_e/10^{20}$, at a time 1.9×10^{-9}s

Fig. 10 — 1μm split selenium foil

19

$$\underset{\sim}{V} \ (t=2.12\times10^{-9} \ s)$$

(a) Velocity field from CASE E, at $t = 2.12 \times 10^{-9}$s

$$\underset{\sim}{V} \ (t=1.9\times10^{-9} \ s)$$

(b) Velocity field from the 1μm split copper foil, at a time 1.9×10^{-9}s
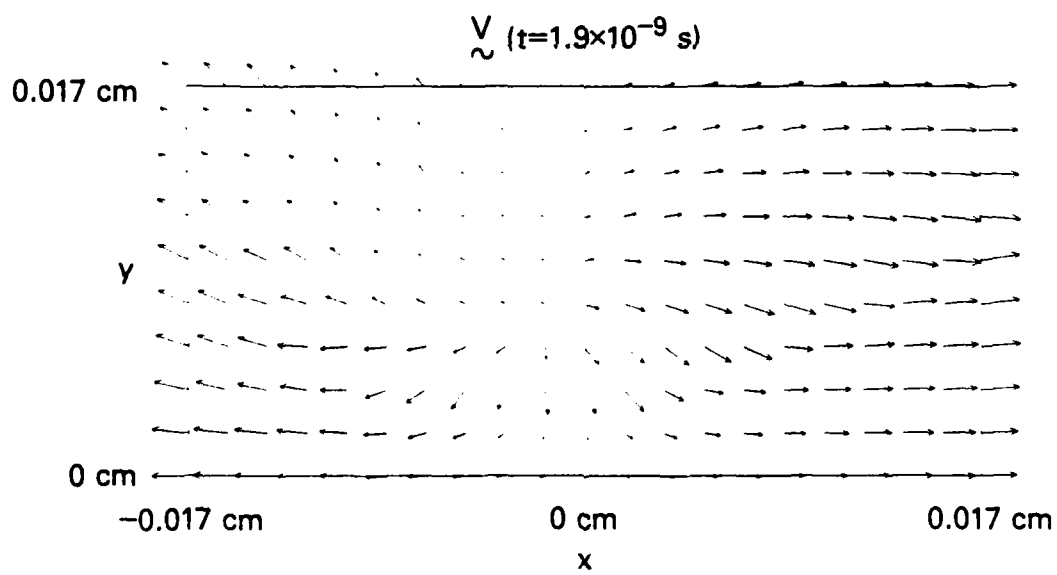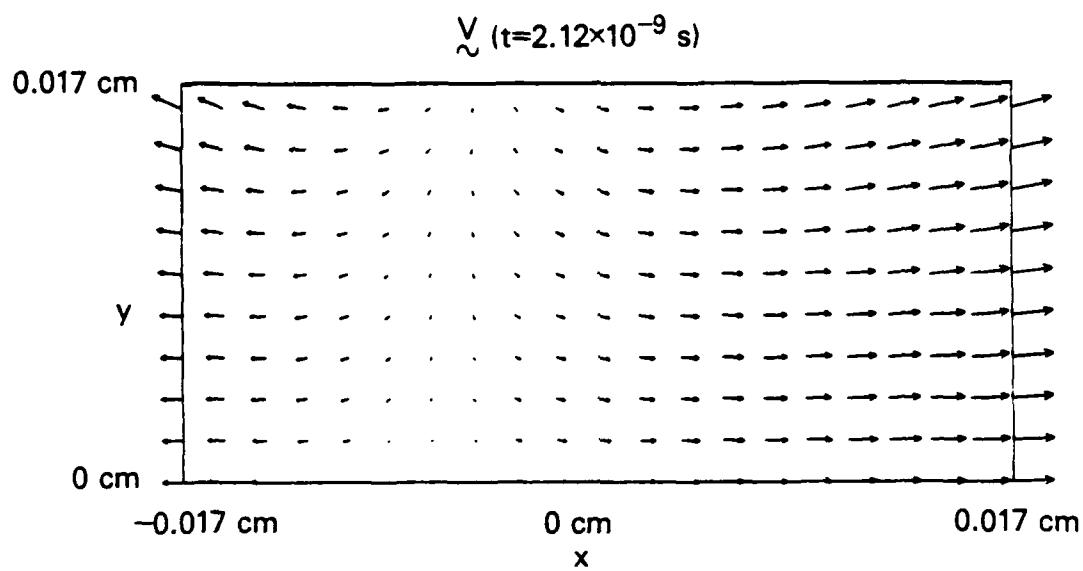
Fig. 11 — Velocity field from simulations with identical incident laser pulses

20

REFERENCES

Boris, J.P. *Naval Research Laboratory Memorandum Report No. 3427*, 37 pages, (1976).

Boris, J.P. and Book, D.L. *J.Comp.Phys.*, **20**, 397-431, (1976) (and references therein).

Boris, J.P. *Comments Plasma Phys. Controlled Fusion* 3, 1, (1977).

Chirkov, V. A. *Sov. J. Quantum Electron.* **14**, 1497, (1984).

Elton, R. C., Molander, W. A. and Lee, T. N. **Proc. Third OSA Topical Conf. on Short Wavelength Coherent Radiation,** *AIP Conf. Proc.* (to be publishe~').

Emery, M.H., Orens, J.H., Gardner, J.H. and Boris, J.P. *Phys.Rev.Lett.* **48**, pp 253-256, (1982).

Feldman, U., Seeley, J. F., and Bhatia, A. K. *J. Appl. Phys.* **56** 2475 (1984).

Lee, T. N., Molander, W. A., Ford, J. L. and Elton, R. C. *Rev. Sci. Instruments* (in press).

London, R. A. and Rosen, M. D. *UCRL Preprint 94085* (1986).

Manheimer, W. M., Colombant, D. G., and Gardner, J. H. *Phys. Fluids* **25** pp. 1644-1652 (1982).

Matthews, D.L., Hagelstein, P.L., Rosen, M.D., Eckart, M.J., Ceglio, N.M., Hazi, A.U., Medecki, H., MacGowan, B.J., Trebes, J.E., Whitten, B.L., Campbell, E.M., Hatcher, C.W., Hawryluk, A.M., Kauffman, R.L., Pleasance, L.D., Rambach, G., Scofield, J.H., Stone, G. and Weaver, T.A. *Phys.Rev.Lett.*, **54**, pp 110-113, (1985).

Orens, J.H. *Naval Research Laboratory Memorandum Report No. 4167*, 20 pages, (1980).

Rosen, M.D., Hagelstein, P.L., Matthews, D.L., Campbell, E.M., Hazi, A.U., Whitten, B.L., MacGowan, B., Turner, R.E. and Lee, R.W. *Phys.Rev.Lett.*, **54**, pp. 106-109 (1985).

END

12-86

DTIC